ISSN 2032-6653

3-phase High Frequency Voltage Input Sensorless Control for Hybrid Electric Vehicle Applications

Nobuyuki Imai*, Shigeo Morimoto**, Masayuki Sanada**, Yoji Takeda**

This paper describes the application of sensorless control for hybrid electric vehicles and an analysis of the influence of magnetic saturation on sensorless control. 3-phase high frequency voltage input sensorless control that provides information on rotor position using a simple integration procedure is proposed. To analyze the influence of magnetic saturation, a non-linear motor voltage equation is solved by using finite element analysis. Simulation results show good correlation with experimental results and clearly reflect the influence of magnetic saturation. The performance of 3-phase high frequency voltage input sensorless control is greatly improved by using analyzed results. The improved sensorless control algorithm is applied to hybrid electric vehicles and gives good startup performance of an internal combustion engine. The proposed approach is very useful for designing control algorithms, considering the influence of magnetic saturation in hybrid electric vehicle applications.

Keywords: **Hybrid electric vehicles, electric drive, sensorless control, interior permanent magnet motor**

1. INTRODUCTION

In terms of high reliability and cost performance, various types of sensorless control algorithms have been proposed. Usually, sensorless control based on variations in inductance is used for applications that require standstill operation [1]-[4]. This type of sensorless control, however, is affected by magnetic saturation. Most of the previous studies have been based on linear models that do not consider magnetic saturation. Hence, magnetic saturation causes significant problems on estimation process of rotor position [5]-[7].

In some hybrid vehicle applications where high torque densities are required, concentrated windings are applied to realize shorter motor lengths. These types of motors are easily affected by magnetic saturation. Therefore, magnetic saturation is unavoidable in these applications. In our previous studies [12]-[16], finite element analysis (FEM) has proved very useful in analyzing the influence of this type of magnetic saturation. And a biased convergent point observer is effective to compensate the influence of magnetic saturation in sensorless control at low speed.

The purpose of this paper is to apply sensorless control to hybrid electric vehicles, and evaluate its performance in the startup operation of an internal combustion engine. Non-linear motor voltage equations and simplified power device models are built into simulation models of MATLAB/Simulink that is a design and simulation tool for control systems. A transient response simulation of sensorless control is performed, and simulation results are compared with experimental results. The validity of the proposed analysis method is confirmed by experimental results.

* Honda R&D Co.,Ltd., 4630 Shimotakanezawa, Haga-machi, Haga-gun, Tochigi 321-3393, JAPAN.
e-mail:Nobuyuki_01_Imai@n.t.rd.honda.co.jp
** Dept. of Electrical and Information Systems Osaka Prefecture University, 1-1 Gakuen-cho, Sakai, Osaka 599-8531, JAPAN.
e-mail:morimoto@eis.osakafu-u.ac.jp, sanada@eis.osakafuu.ac.jp, takeda@eis.osakafu-u.ac.jp

2. 3-PHASE HIGH FREQUENCY VOLTAGE INPUT SENSORLESS CONTROL

A sensorless control algorithm using 3-phase high frequency voltage input is briefly explained [12]-[16]. The phase reluctance values of 3-phase interior permanent magnet synchronous motors (IPMSM) are assumed to be a sinusoidal function of rotor position θ as follows.

$$\begin{cases} R_u = R_m - r\cdot\cos 2\theta \\ R_v = R_m - r\cdot\cos(2\theta - 2\pi/3) \\ R_w = R_m - r\cdot\cos(2\theta + 2\pi/3) \end{cases} \quad (1)$$

where R_u, R_v, R_w are reluctance values of U-phase, V-phase, and W-phase, respectively. R_m is the mean phase reluctance value and r is the amplitude of reluctance variation. The rotor position can be estimated via simple integration using rotating 3-phase high frequency voltage input as follows.

$$\begin{bmatrix} v_{uh} \\ v_{vh} \\ v_{wh} \end{bmatrix} = V_h \left[\sin\omega_h t \quad \sin\left(\omega_h t - \frac{2}{3}\pi\right) \quad \sin\left(\omega_h t - \frac{4}{3}\pi\right) \right]^T \quad (2)$$

ISSN 2032-6653

where V_h is the amplitude of voltage input and ω_h is the angular speed of voltage input, respectively. By processing high frequency currents I_{uh} and I_{wh} that are excited currents of *U*-phase and *W*-phase by injected high frequency voltages, the information on rotor position θ is obtained as follows.

$$I_c = \frac{\omega_h}{\pi}\int_0^{\frac{2\pi}{\omega_h}} \sin 2\omega_h t\left\{\cos\left(\omega_h t + \frac{2}{3}\pi\right)\cdot i_{uh} - \cos\omega_h t \cdot i_{wh}\right\} dt$$

$$= A_t \cos 2\theta \tag{3a}$$

$$I_s = \frac{\omega_h}{\pi}\int_0^{\frac{2\pi}{\omega_h}} \cos 2\omega_h t\left\{\cos\left(\omega_h t + \frac{2}{3}\pi\right)\cdot i_{uh} - \cos\omega_h t \cdot i_{wh}\right\} dt$$

$$= A_t \sin 2\theta \tag{3b}$$

where A_t is a coefficient expressed by

$$A_t = \frac{3\sqrt{3}\Delta l V_h}{4\omega_h\left\{(l-m)^2 - \frac{9\Delta l^2}{4}\right\}} = \frac{\sqrt{3}V_h}{4\omega_h} r \tag{4}$$

l is the mean value of self inductance, m is the mean value of mutual inductance and Δl is the amplitude of variation in inductance, respectively. l, m and Δl are calculated as follows.

$$\begin{cases} l = \dfrac{8R_m N^2}{12R_m^2 - 3r^2} \\ m = -\dfrac{4R_m N^2}{12R_m^2 - 3r^2} \\ \Delta l = \dfrac{4rN^2}{12R_m^2 - 3r^2} \end{cases} \tag{5}$$

Using these I_c and I_s values, rotor position is estimated by a discrete-time observer as follows.

$$\begin{bmatrix} \hat{\theta}(n+1) \\ \hat{\omega}(n+1) \end{bmatrix} = \begin{bmatrix} 1 & \Delta t \\ 0 & 1 \end{bmatrix}\begin{bmatrix} \hat{\theta}(n) \\ \hat{\omega}(n) \end{bmatrix} + \begin{bmatrix} k1 \\ k2 \end{bmatrix}(\Theta_e + \alpha) \tag{6}$$

where Δt, $\hat{\theta}$, $\hat{\omega}$ denote observer sampling time, estimated angle and estimated angular speed, respectively. $k1$ and $k2$ are observer gain values. The convergent point of the observer can be biased by an offset value α that is determined to reduce the angle error caused by magnetic saturation. And approximated angle error Θ_e is obtained as follows.

$$\Theta_e = \begin{cases} \dfrac{I_c \cdot \sin 2\hat{\theta} - I_s \cdot \cos 2\hat{\theta}}{|I_s|} & |I_s| > |I_c| \\ \dfrac{I_c \cdot \sin 2\hat{\theta} - I_s \cdot \cos 2\hat{\theta}}{|I_c|} & |I_c| > |I_s| \end{cases} \tag{7}$$

Θ_e gives an approximation of $\sin 2(\hat{\theta} - \theta) = \sin 2\theta_e$, where θ_e denotes real angle error, and the relation $\Theta_e \approx 2\theta_e$ is established at nearby $\theta_e = 0$deg. As shown in (7), the approximated angle error is normalized. Hence the rotor position can be estimated independently from motor inductance values l, m and Δl.

The block diagram of the proposed 3-phase voltage input sensorless control is shown in Fig. 1.

3. NON-LINEAR ANALYSIS OF MOTOR VOLTAGE EQUATION

When the motor magnetic circuit is saturated, the non-linear motor voltage equation must be solved. In order to solve the non-linear voltage equation, partial differentials of flux-linkage that are calculated considering magnetic saturation are used as follows.

$$\boldsymbol{V} - R\boldsymbol{I} - \frac{\partial \boldsymbol{\Phi}}{\partial t} = \boldsymbol{V} - R\boldsymbol{I} - \frac{\partial \boldsymbol{\Phi}}{\partial \boldsymbol{I}}\frac{d\boldsymbol{I}}{dt} + \frac{\partial \boldsymbol{\Phi}}{\partial \theta}\frac{d\theta}{dt}$$

$$= \boldsymbol{V} - R\boldsymbol{I} - \left(\frac{\partial \boldsymbol{\Phi}}{\partial \boldsymbol{A}}\frac{\partial \boldsymbol{A}}{\partial \boldsymbol{I}}\right)\frac{d\boldsymbol{I}}{dt} - \left(\frac{\partial \boldsymbol{\Phi}}{\partial \boldsymbol{A}}\frac{\partial \boldsymbol{A}}{\partial \theta}\right)\frac{d\theta}{dt} = 0 \tag{8}$$

where $\boldsymbol{\Phi}$ is flux-linkage, $\boldsymbol{A}$ denotes magnetic vector potential, $\boldsymbol{V}$ is a motor voltage vector, $\boldsymbol{I}$ is a motor current vector and R is a motor resistance value, respectively. FEM is very useful in calculating these partial differential values of flux-linkage [11]. As following equation, partial differential values of

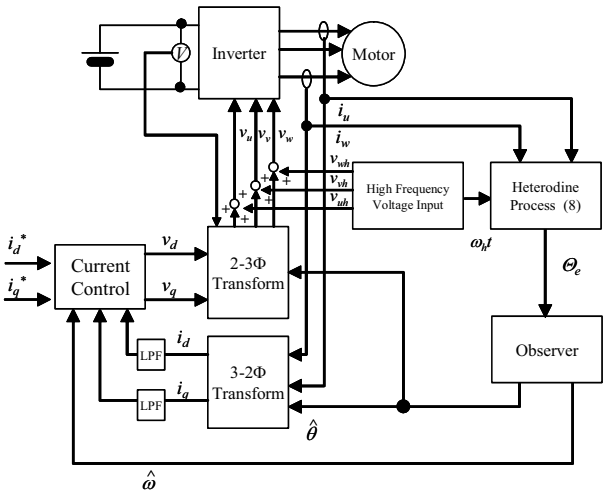

Fig. 1 Block diagram of sensorless control

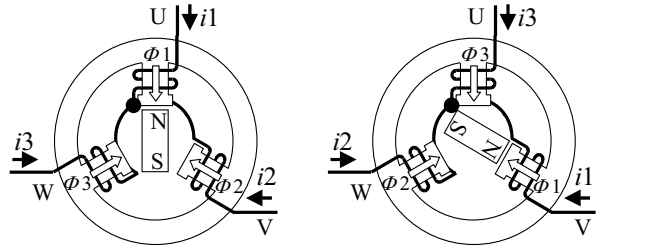

(a) $(\theta, i_u, i_v, i_w)=(\theta 1, i1, i2, i3)$ (b) $(\theta, i_u, i_v, i_w)=(\theta 1+120, i3, i1, i2)$

Fig. 2 Geometric relation of motor magnetic circuit

ISSN 2032-6653

flux-linkage with respect to motor current and angle can be calculated directly.

$$\begin{cases} \left[\dfrac{\partial \Phi}{\partial I} \quad \dfrac{\partial \Phi}{\partial \theta}\right] = \dfrac{\partial \Phi}{\partial A}\left[\dfrac{\partial A}{\partial I} \quad \dfrac{\partial A}{\partial \theta}\right] \\ \left[\dfrac{\partial A}{\partial I} \quad \dfrac{\partial A}{\partial \theta}\right] = \left(\dfrac{\partial G}{\partial A}\right)^{-1}\left[\dfrac{\partial G}{\partial I} \quad \dfrac{\partial G}{\partial \theta}\right] \end{cases} \tag{9}$$

where G is the residual of the Galerkin method. This calculation can be achieved by adding only three column vectors to standard Newton Raphson's methods. However, it is very time-consuming to recalculate these partial differentials according to currents and rotor position. Interpolating the pre-calculated partial differential data table can reduce the calculation time. By selecting calculation points properly, simple interpolations can give good approximations. This type of analysis is well known in the analysis of switched reluctance motors (SRM) [8]-[10].

To reduce calculation points, the symmetry of motor magnetic circuits can be utilized. The motor magnetic circuit of each phase is geometrically shifted 120deg, as shown in Fig. 2. When the rotor position and phase current are shifted 120deg, the flux-linkage of each phase is also shifted 120deg. And north and south poles of the rotor magnet are symmetrical. Hence, the following relation is established.

$$\frac{\partial \Phi_u(\theta 1, i1, i2, i3)}{\partial i_u} = \begin{cases} \dfrac{\partial \Phi_u(\theta 1, i1, i2, i3)}{\partial i_u}, 0 \le \theta 1 < 60 \\ \dfrac{\partial \Phi_w(\theta 1 - 60, -i2, -i3, -i1)}{\partial i_w}, 60 \le \theta 1 < 120 \\ \dfrac{\partial \Phi_v(\theta 1 - 120, i3, i1, i2)}{\partial i_v}, 120 \le \theta 1 < 180 \\ \dfrac{\partial \Phi_u(\theta 1 - 180, -i1, -i2, -i3)}{\partial i_u}, 180 \le \theta 1 < 240 \\ \dfrac{\partial \Phi_w(\theta 1 - 240, i2, i3, i1)}{\partial i_w}, 240 \le \theta 1 < 300 \\ \dfrac{\partial \Phi_v(\theta 1 - 300, -i3, -i1, -i2)}{\partial i_v}, 300 \le \theta 1 < 360 \end{cases} \tag{10}$$

where $\Phi_u(\theta 1, i1, i2, i3)$ denotes the flux-linkage of U-phase at rotor angle $\theta 1$, U-phase current $i1$, V-phase current $i2$ and W-phase current $i3$. Similar relational formulas for Φ_v and Φ_w, are also obtained. By using these relations, the partial differential table data of flux-linkage must be calculated only between rotor angles 0 and 60 deg. The size of the table data is reduced to 1/6.

4. SIMULATION AND EXPERIMENTAL RESULTS

Non-linear simulation of the tested motor is performed by using MATLAB/Simulink.

MATLAB/Simulink is a graphical programming tool that is used in design and simulation of control systems. The non-linear motor voltage equation and simplified power device models are built into MATLAB/Simulink by an s-function block and DLL. Simulating nonlinear electric devices such as diodes or IGBTs precisely is not easy, but detailed characteristics of these devices hardly affect the motor control performance. These switching devices are treated as an ideal switch connected with diodes, and the diode characteristics are approximated by a piece-wise linear function. The transient response analysis of motor drive circuits is realized easily by these approximations and can be executed in a very short time.

Fig. 3 shows the block diagram of the heterodyne process (3) and fig. 4 shows the block diagram of the discrete observer (4), respectively. As shown in these figures, MATLAB/Simulink provides intuitive block diagrams and enables easy implementation of the control algorithm.

4.1 Magnetic Polarity Detection

The inductance value of IPMSM varies in 180deg. cycles. Hence, a sensorless control algorithm using motor saliency cannot specify the magnetic polarity. To specify the magnetic polarity, field current i_d is supplied to the motor [2],[3]. The supplied current causes a field-weakening or field-strengthening effect. In the case of field-strengthening, the motor reluctance increases due to the magnetic saturation. Hence, we can specify the magnetic polarity by measuring the increase in motor reluctance. From (3) and (4), high frequency current amplitude I_p is defined as follows.

$$I_p = \sqrt{I_s^{\,2} + I_c^{\,2}} = \frac{\sqrt{3}\,V_h}{4\omega_h} r \tag{11}$$

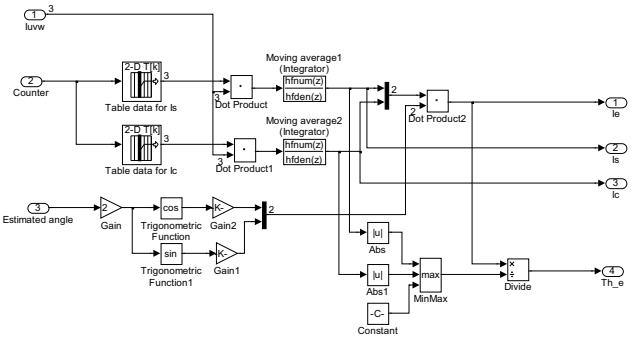

Fig. 3 Block diagram of heterodyne process

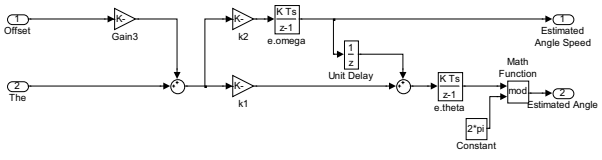

Fig. 4 Block diagram of discrete observer

ISSN 2032-6653

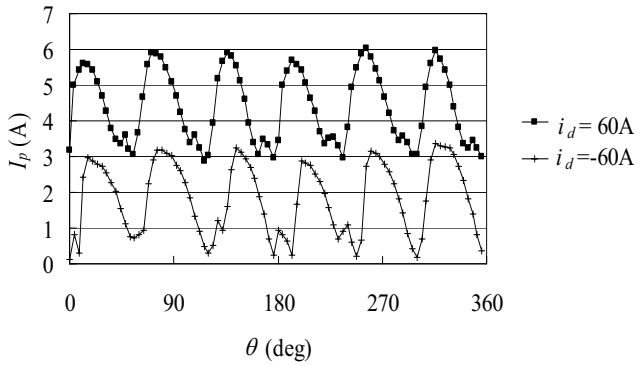

Fig. 5 Rotor angle vs. I_p (simulated)

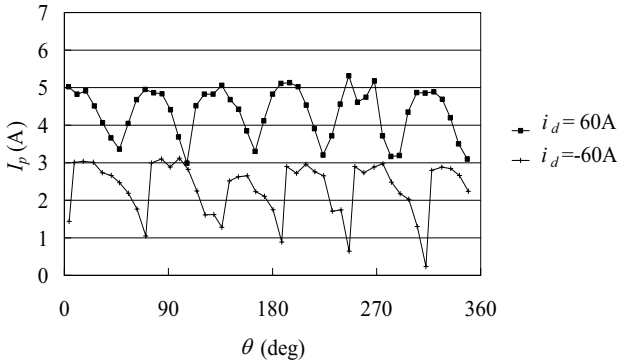

Fig. 6 Rotor angle vs. I_p (measured)

Equation (11) shows that in the case of field-strengthening, I_p increases in accordance with the increase in motor reluctance. Fig. 5 and fig. 6 give examples of magnetic polarity detection. Motor current is controlled by an estimated rotor angle. Fig. 5 shows the simulated I_p values according to rotor angle θ in the case of i_d=60A and id=-60A, respectively. I_p values vary cyclically, with a period of 60deg, and I_p values for i_d =60A are larger than those for i_d=-60A. Fig. 6 shows the experimental results of magnetic polarity detection. Similar to the simulation results, measured I_p values vary cyclically and the values for i_d =60A are larger than those for i_d =-60A. Thus, the simulation results reproduce magnetic saturation well and show good correlation with the experimental results.

4.2 Drive Operation by Sensorless Control at Low Speed

Fig. 7 and fig. 8 show the calculated relationship between the approximated angle error Θ_e and the real angle error θ_e at several rotor positions for i_q=0A and i_q=140A, respectively. Theoretically, the approximated angle error is given by a sinusoidal function of the real angle error as in (7). In the case of i_q=0, the calculated approximated angle error shows an almost sinusoidal wave form. However, due to magnetic saturation, the shape of the approximated angle error for i_q=140A is heavily distorted. The observer converges to the zero

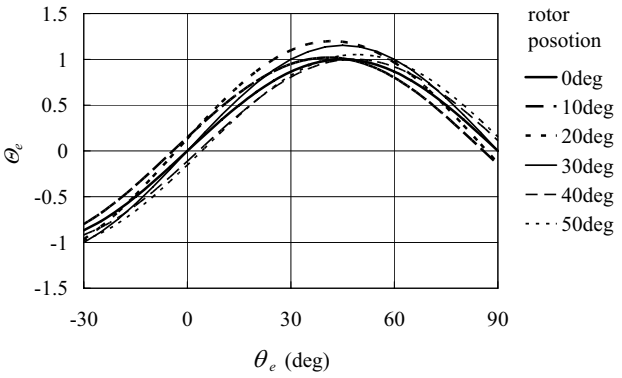

Fig. 7 Calculated Θ_e (i_q=0A, i_d=0A)

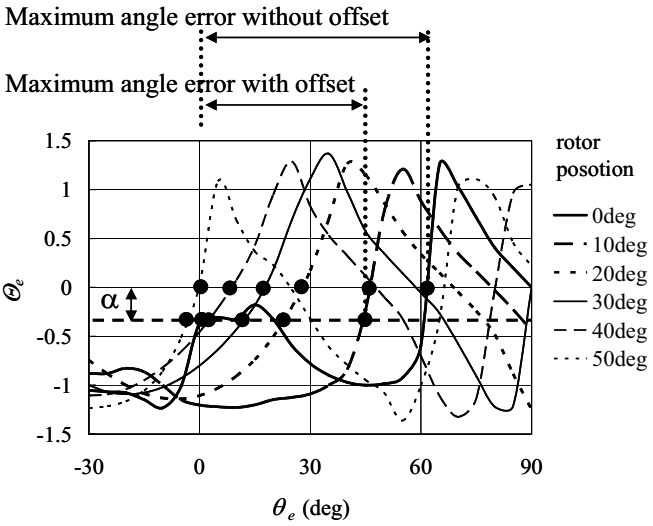

Fig. 8 Calculated Θ_e and convergent points (i_q=140A, i_d=0A)

cross point of each line, hence Fig. 8 means angle error increases especially at around rotor angle θ=0deg. Fig. 9 shows the simulation results of sensorless control for i_q=140A and i_d=0. Fig. 10 shows the experimental results at the same current. Both sets of results show similar tendencies in estimated angle and torque. The estimated angle error increases periodically in 60-deg cycles and motor torque decreases at a rotor position where large estimated angle error exists.

As shown in our previous studies [12]-[16], Fig. 8 denotes that biasing the observer convergent point in the negative direction of Θ_e reduces the estimated angle error. This can be easily achieved by adding positive offset value α to the observer. Fig. 11 shows the simulation results of a biased convergent point observer at i_q=140A. Adding an offset value to the observer, maximum estimated angle error is reduced and the bottom value of motor torque is greatly improved. Fig. 12 shows the experimental results at the same current. Similar to the simulation results, the maximum estimated angle error is reduced and the sharp decline

ISSN 2032-6653

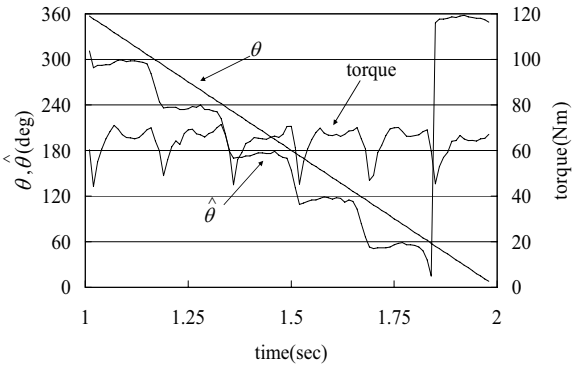

Fig. 9 Estimated angle and torque
(simulated at i_q=140A, i_d=0A, α=0)

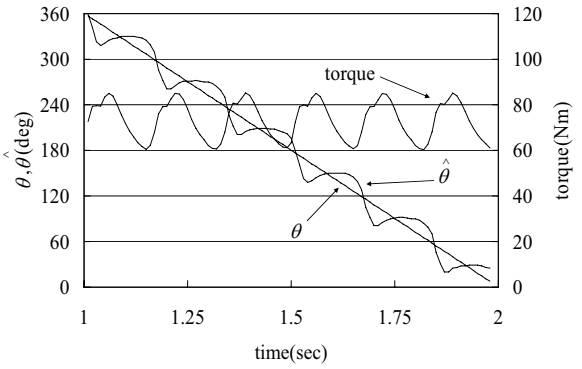

Fig. 11 Estimated angle and torque
(simulated at i_q=140A, i_d=0A, α=0.4)

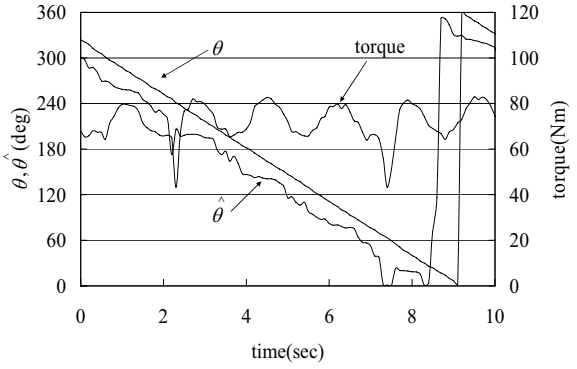

Fig. 10 Estimated angle and torque
(measured at i_q=140A, i_d=0A, α=0)

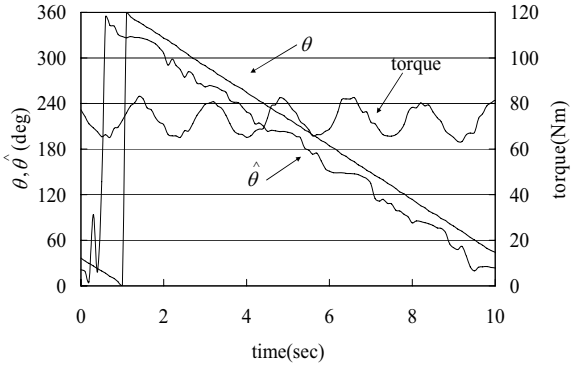

Fig. 12 Estimated angle and torque
(measured at i_q=140A, i_d=0A, α=0.4)

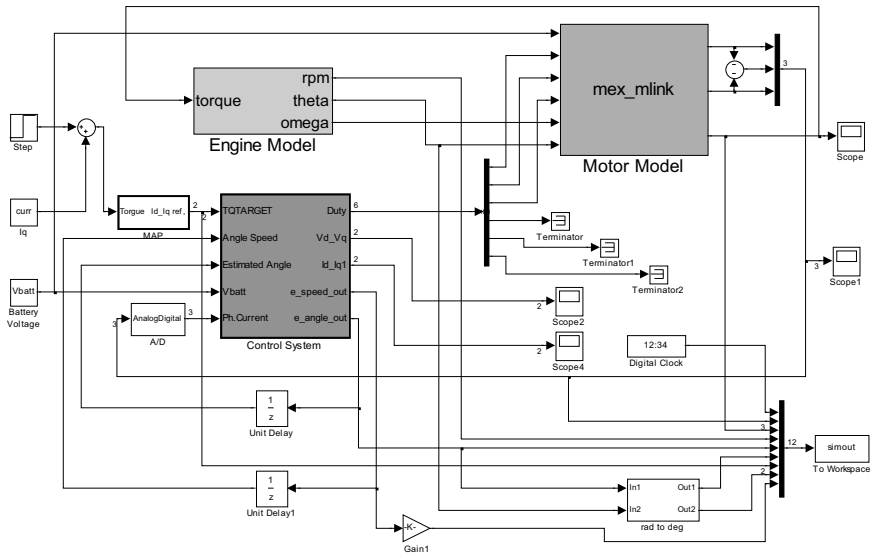

Fig. 13 Simulation model for startup operation of internal combustion engine

of motor torque is well controlled. The bottom value of motor torque increases from about 45Nm to more than 60Nm. Thus, the biased convergent point observer is very effective in reducing the estimated angle error. But the effect of offset value α is very sensitive for some types of IPMSM [16]. To decide the optimal value of α, further consideration is necessary.

4.3 Startup Operation of an Internal Combustion Engine by Sensorless Control

The transient response of the proposed sensorless algorithm is simulated and the proposed algorithm is applied to a mass-produced hybrid electric vehicle. Fig.

ISSN 2032-6653

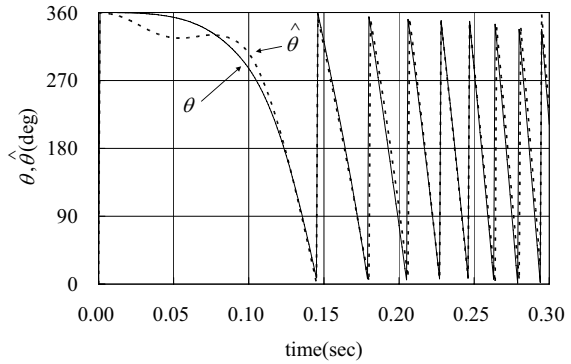

Fig. 14 Simulation results of estimated angle and real angle

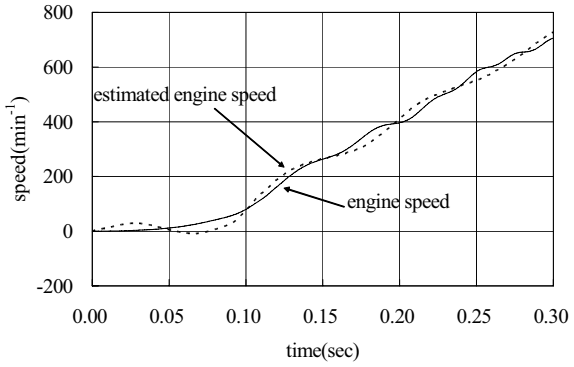

Fig. 15 Simulation results of estimated engine speed and real engine speed

13 shows the MATLAB/Simulink block diagram for the transient analysis. The model comprises a simplified engine model, a control system and a motor model as described by an s-function block diagram. Fig. 14 shows simulation results of estimated angle and real angle values for startup operation by sensorless control. Fig. 15 shows simulation results of the estimated engine speed and real engine speed for startup operation by sensorless control. From these results, the internal combustion engine is accelerated smoothly and rapidly. The estimated angle and estimated engine speed follow the real angle and actual engine speed well while accelerating. These results show good tracking performance of the proposed sensorless control algorithm. Fig. 16 shows experimental results of the estimated angle and estimated engine speed. The test vehicle only is equipped with low resolution pulse sensors for motor control. Therefore, only the estimated angle and estimated engine speed are available at startup operation. Similar to simulation results, the internal combustion engine is accelerated smoothly and rapidly. These simulation and experimental results confirm the validity of the proposed analysis methods**.**

5. CONCLUSION

An analysis method for 3-phase high frequency voltage input sensorless control that considers the influence of magnetic saturation is proposed. Using FEM analysis, partial differential values of flux-linkage can be calculated directly and precisely in a short time. High-speed analysis is realized by interpolating the table data of calculated partial differential values and using simplified power device models. The geometric relation of motor magnetic circuits and the redundancy of motor current help reduce table data calculation points. Simulation results show good correlation with experimental results and reflect the influence of magnetic saturation well. The performance of 3-phase high frequency voltage input sensorless control is greatly improved using the analyzed results. The improved sensorless control algorithm is applied to hybrid electric vehicles and gives good startup performance of an internal combustion engine. The proposed method can be very useful in designing control algorithms considering the influence of magnetic saturation in hybrid electric vehicle applications.

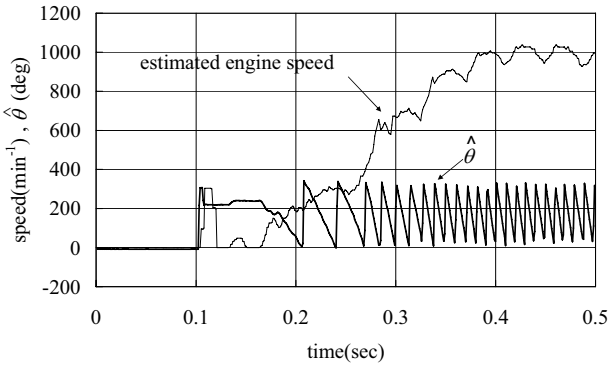

Fig. 16 Experimental results for startup operation of internal combustion engine

REFERENCES

[1] M. J. Corley, R. D. Lorenz, “Rotor Position and Velocity Estimation for a Salient-Pole Permanent Magnet Synchronous Machine at Standstill and High Speeds”, IEEE Trans. Ind. Appl., vol. 34, pp.784-789, Jul./Aug. 1998.

[2] T. Aihara, T. Yanase, A. Mashimo, K. Endo, “Sensorless Torque Control of Salient-Pole Synchronous Motor at Zero-Speed Operation”, IEEE Trans. Power Electron., vol. 14, pp.202-208, Jan. 1999

[3] T. Noguchi, K. Yamada, S. Kondo, I. Takahashi, “Initial Rotor Position Estimation Method of Sensorless PM Synchronous Motor with No Sensitivity to Armature Resistance”, IEEE Trans. Ind. Appl., vol. 45, pp.118-125, Feb. 1998

[4] S. Shinnaka, “New “Mirror-Phase Vector Control” for Sensorless Drive of Permanent-Magnet Synchronous Motor With Pole Saliency”, IEEE Trans. Ind. Appl., vol. 40, pp.599-606, Mar./Apr. 2004.

[5] M. W. Degner, R. D. Lorenz, “Using Multiple Saliencies for the Estimation of Flux, Position, and Velocity in AC Machines”, IEEE Trans. Ind. Appl., vol. 34, pp.1097-1104,

ISSN 2032-6653

Sept./Oct.1998
[6] Nicola Bianchi, Silverio Bolognani, “Influence of Rotor Geometry of an Interior PM Motor on Sensorless Control Feasibility”, Proc. IEEE Ind. App. Soc. Annual Meeting, Oct. 2005.
[7] Paolo Guglielmi, Michele Pastorelli, Alfredo Vagati, “Cross saturation effects in IPM motors and related impact on zero-speed sensorless control”, Proc. IEEE Ind. App. Soc. Annual Meeting, Oct. 2005.
[8] G. S. Buja, M. I. Valla, “Control Characteristics of a SRM drive taking into account the motor saturation”, in Proc. IECON’90, pp.1013-1021, 1990
[9] R. Krishnan, R. A. Bedingfield, “Dynamic analysis of an SRM drive system”, in Conf. Rec. IEEE-IAS Annu. Meeting, pp.265-271, 1991
[10] A. V. Radun, “Design consideration for the switched reluctance motor”, in Conf. Rec. IEEE-IAS Annu. Meeting, pp.290-297, 1994
[11] T.Nakata, N. Takahashi, K. Fujiwara, A. Ahagon, “3-D Finite Element Method for Analyzing Magnetic Field in Electrical Machines Excited from Voltage Source”, IEEE Trans. Magn., vol.24, pp.2582-2584, Nov. 1988.
[12] N. Imai, S. Morimoto, Y. Takeda, “Error Analysis of Sensorless Control for Permanent Magnet Synchronous Motors using Finite Element Method”, IEEJ The Papers of Joint Technical Meeting on Static Apparatus and Rotating Machinery, SA-04-14, RM-04-14, pp.1-6, 2004. [in Japanese]
[13] N. Imai, S. Morimoto, M. Sanada, Y. Takeda, “Influence of Magnetic Saturation on Sensorless Control for Permanent Magnet Synchronous Motors”, IEEJ The Papers of Joint Technical Meeting on Rotating Machinery, RM-04-59, pp.1-6, 2004. [in Japanese]
[14] N. Imai, S. Morimoto, M. Sanada, Y. Takeda, “High-Speed Analysis of 3-phase High Frequency Voltage Input Sensorless Control Fed by PWM Inverters Considering Magnetic Saturation”, in Proc. IPEC2005, pp.2221-2227, 2005
[15] N. Imai, S. Morimoto, M. Sanada, Y. Takeda, “Influence of Magnetic Saturation on 3-phase High Frequency Voltage Input Sensorless Control for IPMSM”, IEEJ Trans. IA, vol.125, pp.659-665, Apr. 2005. [in Japanese]
[16] N. Imai, S. Morimoto, M. Sanada, Y. Takeda, “Influence of PM Flux Variation and Magnetic Saturation on Sensorless Control for Interior Permanent Magnet Synchronous Motors”, Proc. IEEE Ind. App. Soc. Annual Meeting, Oct. 2005.

BIOGRAPHIES

Nobuyuki Imai was born in Japan in 1962. He received his B.E. and M.E.degrees in system engineering from Kobe University in 1985 and 1987, respectively. He joined Honda R&D Co., Ltd. in 1987. He is engaged in research and development of hybrid vehicles. His research interests include analysis and control of synchronous motors. He is a member of the Society of Instrument and Control Engineers and the Institute of Electrical Engineering Japan.

Shigeo Morimoto was born in Japan in 1959. He received his B.E., M.E. and Ph.D degrees from Osaka Prefecture University, Sakai, Japan, in 1982, 1984, and 1990, respectively. He joined Mitsubishi Electric Corporation, Tokyo, Japan, in 1984. Since 1988, he has been with the Department of Electrical and Information Systems, Osaka Prefecture University, where he is currently an Associate Professor. He has been engaged in research on AC drive systems and motion control. Dr. Morimoto is a Member of the IEEE, the Society of Instrumental and Control Engineers of Japan, the Institute of Systems, Control and Information Engineers, and the Japan Institute of Power Electronics.

Masayuki Sanada was born in Japan in 1966. He received his B.E., M.E., and Ph.D degrees from Osaka Prefecture University, Sakai, Japan, in 1989 and 1991, and 1994, respectively. In 1994, he joined the Department of Electrical and Information Systems, Osaka Prefecture University, where he is currently an Assistant Professor. His main areas of research are linear motors for direct drive applications and their control systems. Dr. Sanada is a Member of the IEEE, the Japan Institute of Power Electronics, and the Japan Society of Applied Electromagnetics and Mechanics.

Yoji Takeda was born in Japan in 1943. He received his B.E., M.E., and Ph.D degrees from Osaka Prefecture University, Sakai, Japan, in 1966, 1968, and 1977, respectively. Since 1968, he has been with the Department of Electrical and Information Systems, Osaka Prefecture University, where he is currently a Professor. His main areas of research are permanent magnet synchronous motors, linear motors, and their control systems. Dr. Takeda is a Member of the IEEE, the Institute of Systems, Control and Information Engineers, and the Japan Institute of Power Electronics.